Journal of Alloys and Compounds 509 (2011) 5309–5314

Contents lists available at ScienceDirect

Journal of Alloys and Compounds

journal homepage: www.elsevier.com/locate/jallcom

Structural and electrochemical hydrogen storage properties of Mg_2Ni-based alloys

Yunfeng Zhu*, Chen Yang, Jinyu Zhu, Liquan Li

College of Materials Science and Engineering, Nanjing University of Technology, 5 Xinmofan Road, Nanjing 210009, People's Republic of China

ARTICLE INFO

Article history:
Received 22 December 2010
Received in revised form 1 February 2011
Accepted 1 February 2011
Available online 17 February 2011

Keywords:
Hydrogen storage alloy
Mg_2Ni alloy electrode
HCS + MM
Electrochemical properties

ABSTRACT

Four different methods, i.e. hydriding combustion synthesis + mechanical milling (HCS + MM), induction melting (followed by hydriding) + mechanical milling (IM(Hyd) + MM), combustion synthesis + mechanical milling (CS + MM) and induction melting + mechanical milling (IM + MM), were used to prepare Mg_2Ni-based hydrogen storage alloys used as the negative electrode material in a nickel–metal hydride (Ni/MH) battery. The structural and electrochemical hydrogen storage properties of the Mg_2Ni-based alloys have been investigated systematically. The XRD results indicate that the as-milled products show nanocrystalline or amorphous-like structures. Electrochemical measurements show that the as-milled hydrides exhibit higher discharge capacity and better electrochemical kinetic property than the as-milled alloys. Among the four different methods, the HCS + MM product possesses the highest discharge capacity (578 mAh g^{-1}), the best high rate dischargeability (HRD) and the highest exchange current density (58.8 mA g^{-1}). It is suggested that the novel method of HCS + MM is promising to prepare Mg-based hydrogen storage electrode alloy with high discharge capacity and activity.

1. Introduction

At present, nickel–metal hydride (Ni/MH) batteries using hydrogen storage alloys as negative electrode material are widely applied in many fields, from cellphone to hybrid electric vehicles (HEVs), owing to their superior charge/discharge characteristics and environmental friendliness [1–16]. However, the commercial negative electrode materials ($LaNi_5$-based alloys and RMgNi alloys, R = rare earth metals) are facing challenges for their unsatisfactory theoretical specific capacities and high cost. Thus, it is important to develop other materials with higher discharge capacity and low cost.

Mg_2Ni, a typical A_2B type hydrogen storage alloy, has been attracting people's attention for its high theoretical capacity (999 mAh g^{-1}), low weight, low cost and pollution-free nature [17]. Nonetheless, the high deterioration rate in alkaline electrolyte and the low practical electrochemical capacity limit the application of Mg_2Ni alloy in Ni/MH battery systems. Various methods have been studied to improve the electrochemical performance of the Mg_2Ni alloy, including refinements of bulk structure [18,19], elemental substitution [20–22], surface treatment [23–25], composite treatment [26–28] and novel preparation methods like isothermal evaporation casting process [29], cold rolling [30,31] and polyol reduction [32].

A novel method called hydriding combustion synthesis (HCS) is developed specially to synthesize Mg-based hydrogen storage alloys directly from powders under pressurized hydrogen. The HCS has the advantages of short preparation time, low energy consumption and high activity of the product [33–35]. Another method called mechanical milling (MM) has been widely used to prepare Mg-based materials with nanocrystalline and amorphous structures, which are favorable for hydrogen absorption and desorption [36–38]. Especially, hydrogen can be absorbed/desorbed electrochemically by the Mg-based electrode alloys with nanocrystalline and amorphous structures [17]. An innovative method integrating HCS and MM has been proposed in our previous work to produce Mg-based hydrogen storage alloy, and the product prepared by HCS + MM exhibits excellent gaseous hydrogen storage properties [39,40].

In this paper, we investigate systematically the structural and electrochemical hydrogen storage properties of the Mg_2Ni-based alloy electrodes prepared by four different methods of HCS + MM, IM(Hyd) + MM, CS + MM and IM + MM. The aim of this paper is to verify whether the method of HCS + MM is suitable for preparing Mg-based hydrogen storage electrode alloy by comparing with other preparation methods.

2. Experimental

2.1. Sample preparation

The HCS product was prepared from commercial Mg (99.9 wt.% in purity and <150 μm in particle size) and Ni (99.7 wt.% in purity and 2–3 μm in particle size)

* Corresponding author. Tel.: +86 25 83587242.
E-mail address: yfzhu@njut.edu.cn (Y. Zhu).

0925-8388/$ – see front matter © 2011 Elsevier B.V. All rights reserved.
doi:10.1016/j.jallcom.2011.02.017

powders. The powders were mixed by an ultrasonic homogenizer in acetone for 1 h. As opposed to our previous study, the molar ratio of Mg:Ni is 2.1:1 instead of 2:1 for part of Mg will be evaporated during the HCS process [40]. The XRD result shows that the HCS product is composed of pure Mg_2Ni hydrides and no Ni or $MgNi_2$ is found. After being completely dried in air, the well-mixed powder was placed directly into the synthesis reactor without compacting. Before heating, the reactor was evacuated by a rotary pump, then argon at 0.1 MPa was introduced and the reactor was evacuated again. This cleaning procedure was repeated twice to remove any oxygen in the system. During HCS process, the mixed powder was heated from room temperature to 850 K at the rate of 7 K min^{-1} and held for 1 h under 1.9 MPa hydrogen pressure. Subsequently, the sample was cooled down under hydrogen atmosphere. The CS product was prepared with the similar process except that the sample was synthesized under 0.1 MPa Ar atmosphere.

The IM product was prepared by induction melting of Mg and Ni metals (99.9 wt.% in purity) on a water-cooled copper crucible under argon atmosphere. The ingot was turned over and remelted twice for homogeneity. During melting, excess Mg was added into the crucible to compensate the evaporation loss of Mg during induction melting. The XRD result shows that the IM product consists of a single phase of Mg_2Ni. Then part of the alloy was mechanically crushed and ground to powders of 100 mesh size for further hydriding and mechanical milling process. During hydriding, the Mg_2Ni was first hydrogenated at 573 K under 2.0 MPa hydrogen pressure for 2 h, and then dehydrogenated at 573 K under vacuum. The process was repeated three times for full activation. Finally, the sample was hydrogenated at 573 K under 2.0 MPa hydrogen pressure for 2 h. The as-prepared sample was denoted as IM(Hyd) product.

Part of the products prepared by HCS, IM(Hyd), CS and IM were further treated by mechanical milling with 3 wt.% (*vs.* the product) graphite for 5 h at a speed of 400 rpm and 40:1 in ball-to-powder ratio using a planetary-type ball mill under 0.1 MPa argon atmosphere, respectively. The graphite was added as the process control agent (PCA) for improving the milling efficiency. The as-milled products were denoted as HCS + MM, IM(Hyd) + MM, CS + MM and IM + MM product, respectively.

2.2. Sample characterization

All the testing electrodes were prepared as follows: 0.1 g alloy powder was mixed with 0.4 g carbonyl nickel powder and then cold-pressed into a pellet of 10 mm diameter and 1 mm thickness under a pressure of 12 MPa. Electrochemical measurements were performed at 30 ± 1 °C in 6 M KOH aqueous solution using a three-electrode cell. The working electrode is the testing electrode, the counter electrode is a sintered $Ni(OH)_2$/NiOOH electrode and the reference electrode is Hg/HgO electrode. The discharge capacity and the electrochemical cycle stability were determined by the galvanostatic method. The hydride electrodes were first discharged at 30 mA g^{-1} to the cut-off potential of −0.6 V *vs.* the Hg/HgO reference electrode, and then charged at 300 mA g^{-1} for 2 h after 10 min rest. The alloy electrodes were first charged at 300 mA g^{-1} for 2 h and then discharged at 30 mA g^{-1} to the cut-off potential of −0.6 V *vs.* the Hg/HgO reference electrode after 10 min rest. The discharge capacities of electrodes were evaluated by the amount of active substances. To investigate the high rate dischargeability (HRD) of the alloy electrodes, discharge capacities at different discharge current densities (100, 200, 400 mA g^{-1}) were measured for the first cycle.

Linear polarization curves were measured at a scanning rate of 0.1 mV s^{-1} from −5 to 5 mV (*vs.* open circuit potential) at 50% depth of discharge (DOD). Tafel polarization curves were measured at a scanning rate of 1 mV s^{-1} from −300 to 300 mV (*vs.* open circuit potential) at 100% DOD. Electrochemical impedance spectroscopy (EIS) studies of the electrodes were performed in a frequency range of 100 kHz to 5 mHz with an AC amplitude of 5 mV at 50% DOD under open-circuit conditions, using ZPLOT electrochemical impedance software. For the potentiostatic discharge, the electrodes were discharge at +600 mV (*vs.* open circuit potential) potential step and 100% depth of charge (DOC) for 3600 s. The above electrochemical tests were performed at room temperature in the 6 M KOH aqueous solution on a CHI660C electrochemical workstation.

The phase structures of the samples were characterized by X-ray diffraction (XRD) on an ARL X'TRA diffractometer with Cu K_α radiation. The morphologies of the samples were analyzed by a JSM-6360LV scanning electron microscopy (SEM). The particle size of the powder samples were examined by a NSKC-1 type particle size analyzer.

3. Results and discussion

Fig. 1 shows the XRD patterns of the samples prepared by HCS, IM(Hyd), CS and IM. As shown in Fig. 1(a) and (b), both of the HCS and IM(Hyd) products are composed of the main phase Mg_2NiH_4 and trace of $Mg_2NiH_{0.3}$. For the HCS product, owing to the addition of excessive Mg (Mg/Ni = 2.1) during the HCS process, no Ni or $MgNi_2$ phase can be found. The appearance of $Mg_2NiH_{0.3}$ indicates incomplete hydrogenation of Mg_2Ni. As shown in Fig. 1(c) and (d), both of the CS and IM products are composed of the single phase Mg_2Ni.

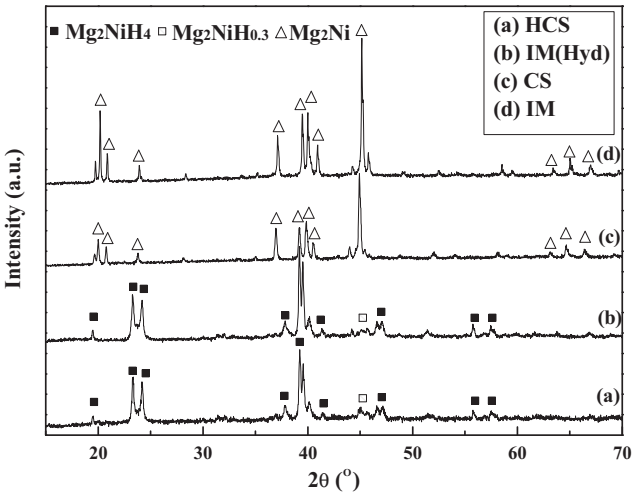

Fig. 1. XRD patterns of the samples prepared by HCS, IM(Hyd), CS and IM.

Fig. 2 shows the XRD patterns of the samples prepared by HCS + MM, IM(Hyd) + MM, CS + MM and IM + MM. As expected, the sharp diffraction peaks are broadened significantly and the peak intensities are also decreased after mechanical milling for 5 h, showing nanocrystalline or amorphous-like structure of the products. In Fig. 2(a) and (b), most of the Mg_2NiH_4 peaks almost disappear, while the intensities of $Mg_2NiH_{0.3}$ peaks are increased significantly as compared to the sample before milling, which can be attributed to two reasons: (1) nanocrystallization or amorphization of Mg_2NiH_4 is easily obtained during mechanical milling as it is more brittle than $Mg_2NiH_{0.3}$ [39]; (2) part of Mg_2NiH_4 was dehydrogenated during the MM process. Besides, $Mg(OH)_2$ peaks were detected in the products due to exposure of the samples to air. In Fig. 2(c) and (d), the peaks of Mg_2Ni are also broadened significantly after mechanical milling, indicating an increase in microstrain and a decrease in crystallite size.

The SEM micrographs of the samples prepared by HCS + MM, IM(Hyd) + MM, CS + MM and IM + MM are shown in Fig. 3. The average particle size of the samples was examined to be around 1.0, 1.2, 2.4 and 1.8 μm for the HCS + MM, IM(Hyd) + MM, CS + MM and IM + MM products, respectively. It can be seen that the HCS + MM and IM(Hyd) + MM products possess smaller particle size than that

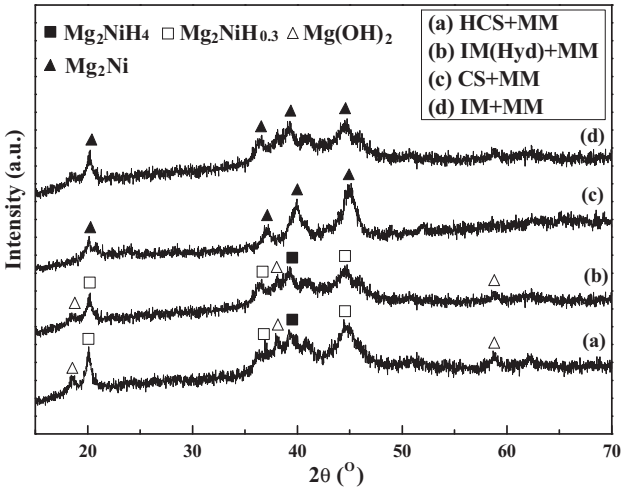

Fig. 2. XRD patterns of the samples prepared by HCS + MM, IM(Hyd) + MM, CS + MM and IM + MM.

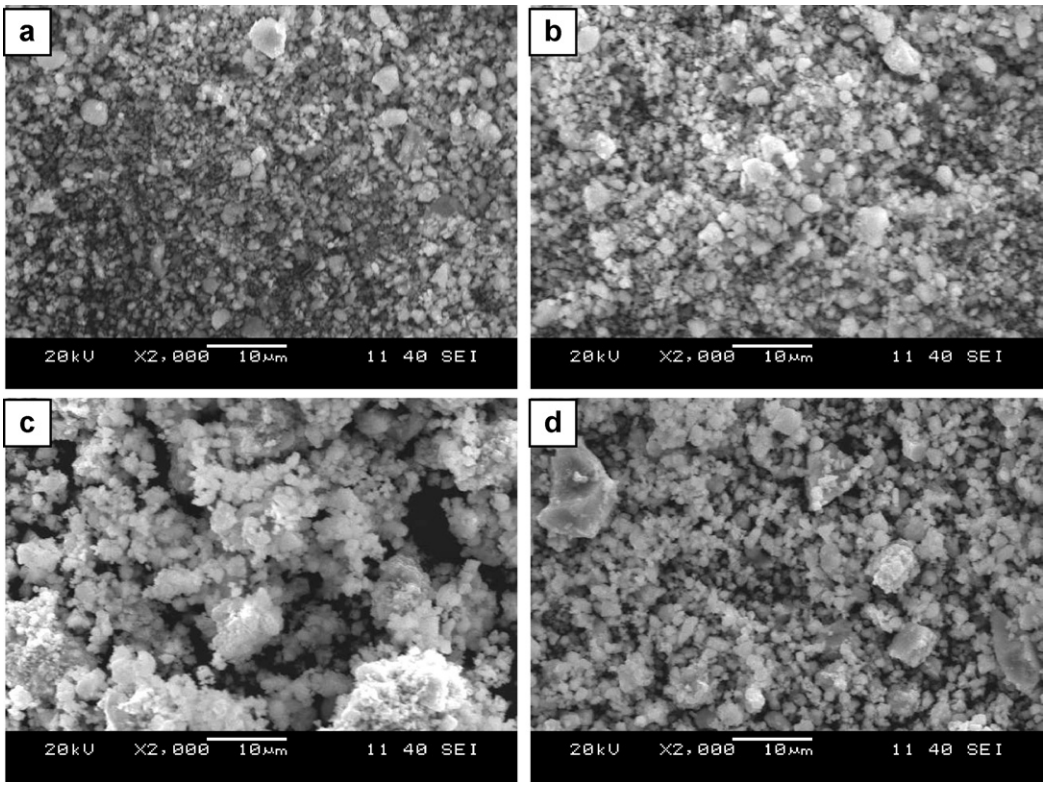

Fig. 3. SEM micrographs of the samples prepared by HCS + MM (a), IM(Hyd) + MM (b), CS + MM (c) and IM + MM (d).

of the CS + MM and IM + MM products, which can be attributed to two factors. On the one hand, the CS and IM products are composed of Mg_2Ni alloy, whereas the HCS and IM(Hyd) products are composed of Mg_2Ni hydrides, which have been pulverized upon hydrogenation due to the large volume expansion. On the other hand, the milling efficiency of Mg_2Ni hydrides is better than that of Mg_2Ni alloy due to their brittle nature. Moreover, large agglomerates can be found in the CS + MM product (Fig. 3(c)) and the IM + MM product (Fig. 3(d)) in spite of the addition of graphite during mechanical milling. Therefore, the HCS + MM and IM(Hyd) + MM products have a smaller and more homogeneous particle size, which is favorable to the electrochemical performance.

Fig. 4 shows the discharge curves of the first cycle for the electrodes prepared by different methods. The discharge capacities are listed in Table 1. It can be seen that the curves can be classified into two types: one is for the HCS + MM and IM(Hyd) + MM products, and the other is for the CS + MM and IM + MM products. The HCS + MM and IM(Hyd) + MM products reveal a flat potential plateau at the initial stage of discharging and a sloping potential plateau at the following discharge stage. The CS + MM and IM + MM products only show one sloping and more positive potential plateau, which is similar to the conventional Mg-based hydrogen storage electrode alloy. As the HCS + MM and IM(Hyd) + MM products are composed of Mg_2Ni hydrides with nanocrystalline or amorphous structures, the formation of the two discharge plateaus is still unclear at present and needs further investigation. Obviously, the HCS + MM and IM(Hyd) + MM products have higher discharge capacity than that of the CS + MM and IM + MM products. The HCS + MM product shows the highest discharge capacity of 578 mAh g^{-1}. As mentioned above, the HCS + MM and IM(Hyd) + MM products have smaller particle size than the CS + MM and IM + MM products, which is beneficial to hydrogen diffusion in the alloy electrodes during discharging. Besides, a smaller particle size of Mg_2Ni hydrides with larger surface areas leads to a smaller current density on the particle surface, which reduces the electrochemical polarization and hence increases the discharge plateau (more negative potential) [41]. These two factors may be responsible for higher discharge capacity of the HCS + MM and IM(Hyd) + MM products.

The evolution of the discharge capacity of the electrodes with cycle number is shown in Fig. 5. The capacity retention rate R_8 (C_8/C_{max}) is also listed in Table 1. Although the HCS + MM product has the highest discharge capacity, it undergoes rapid degradation in discharge capacity similar to the other samples. We have examined the phase structure of the HCS + MM product by XRD during charging/discharging. It was found that the nanocrystalline or amorphous-like structure of the product was stable during cycling. However, the amount of $Mg(OH)_2$ was increased rapidly,

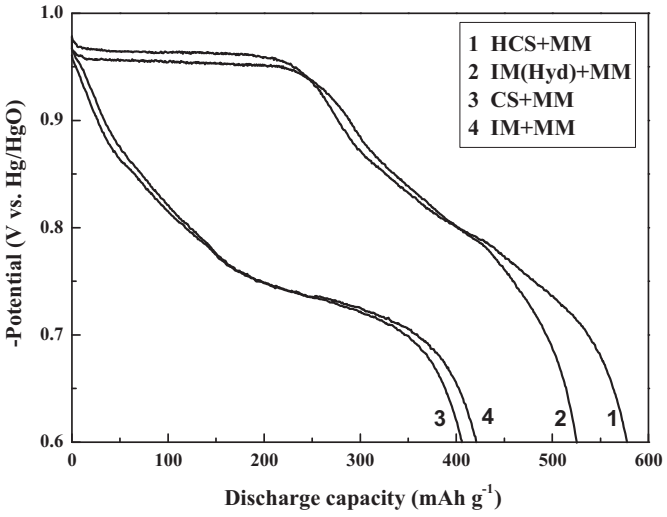

Fig. 4. Discharge curves of the different samples measured at 303 K (discharge rate: 30 mA g^{-1}; the first cycle).

Table 1
The electrochemical properties of the samples prepared by HCS + MM, IM(Hyd) + MM, CS + MM and IM + MM.

Samples	C_{max} (mAh g^{-1})	R_8 (%)	E_{corr} (V)	I_0 (mA g^{-1})	R_{ct} (mΩ)	D/a^2 ($\times 10^{-5}$ s^{-1})
HCS + MM	578	6.9	−0.954	58.8	280	1.67
IM(Hyd) + MM	525	5.2	−0.942	51.7	340	1.66
CS + MM	406	11.3	−0.889	29.6	1060	1.44
IM + MM	421	10.1	−0.846	24.0	1370	1.32

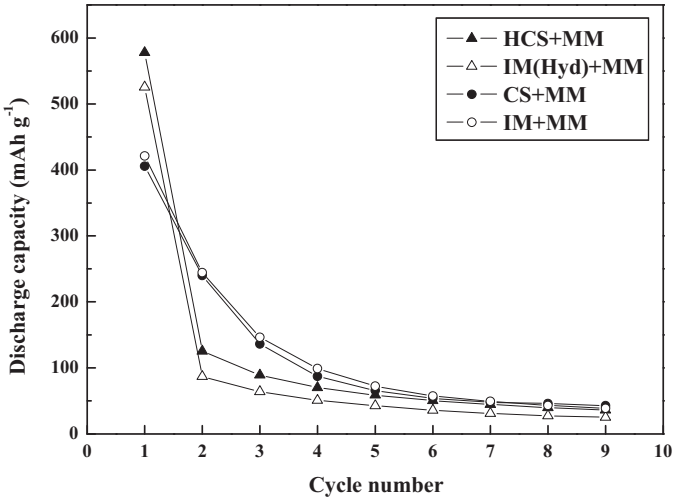

Fig. 5. Discharge capacities as a function of cycle number for the different samples measured at 303 K.

leading to the decrease in the amount of active substance for hydrogenation/dehydrogenation, and therefore a decreased discharge capacity of the electrode. Thus, the corrosion of Mg in alkaline solution during charging/discharging is responsible for the poor cycle life of the electrode [42]. Besides, as the HCS + MM and IM(Hyd) + MM products have smaller particle size and larger surface areas, they have a worse cycling stability than the CS + MM and IM + MM products. For studying the anti-corrosion ability of the different electrodes, Tafel polarization test was performed. The Tafel polarization curves of the different electrodes are shown in Fig. 6 and the corrosion potential E_{corr} is listed in Table 1. It can be seen that the corrosion potentials of the CS + MM and IM + MM products are higher than those of the HCS + MM and IM(Hyd) + MM products, indicating that the CS + MM and IM + MM products have a better anti-corrosion ability, and thus a better cycling stability.

Fig. 7 shows the high rate dischargeability (HRD) of the different electrodes. The HRD is calculated from the following formula:

$$\mathrm{HRD} = \frac{C_d}{C_d + C_{60}} \times 100\% \quad (1)$$

where C_d is the discharge capacity with cut-off potential of −0.6 V (*vs.* Hg/HgO) at the discharge current density I_d (100, 200, 400 mA g^{-1}), C_{60} is the residual discharge capacity with the same cut-off potential at the discharge current density I (60 mA g^{-1}) after the alloy electrode has been fully discharged at the discharge current density I_d. It can be found that the HCS + MM and IM(Hyd) + MM products have better HRD and hence better electrochemical kinetics than the CS + MM and IM + MM products. Moreover, the HCS + MM product possesses the best HRD among the four samples. It has been reported that the HRD of the MH electrode is mainly determined by charge-transfer on the alloy surface and hydrogen diffusion inside the alloy [43]. In order to understand further the electrochemical kinetic property of the different electrodes, linear polarization, EIS and potentiostatic discharge tests were performed.

Fig. 8 shows the linear polarization curves of the different electrodes. The exchange current density I_0 of the electrode is an important parameter for evaluating the rate of charge-transfer on the alloy surface. When the overpotential is varied within a small scope, the exchange current density can be calculated from the following formula [44]:

$$I_0 = \frac{RTI}{F\eta} \quad (2)$$

where R is the gas constant, T is the absolute temperature (K), I is the applied current density (mA g^{-1}), F is the Faraday constant and η is the total overpotential (mV). The calculated I_0 values are listed in Table 1. It is obvious that the I_0 of the HCS + MM and IM(Hyd) + MM products is larger than that of the CS + MM and IM + MM products, and the HCS + MM product has the largest I_0. The larger I_0 of the HCS + MM and IM(Hyd) + MM products may result from their structural characteristics, and the smaller particles can enhance the

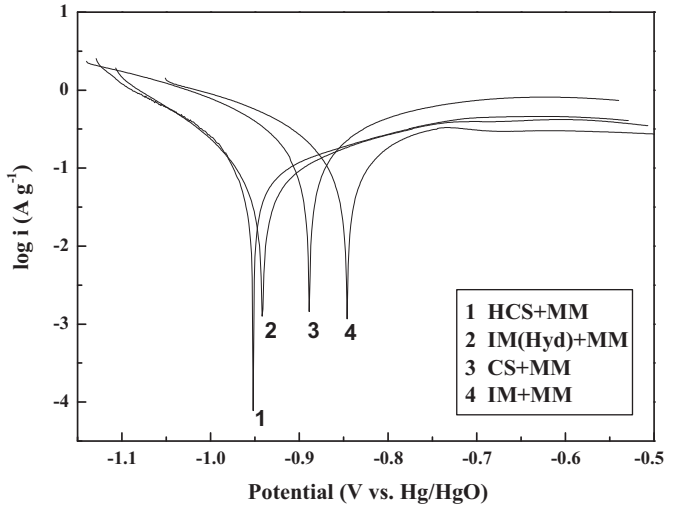

Fig. 6. Tafel polarization curves of the different samples (scan rate: 1 mV s^{-1}).

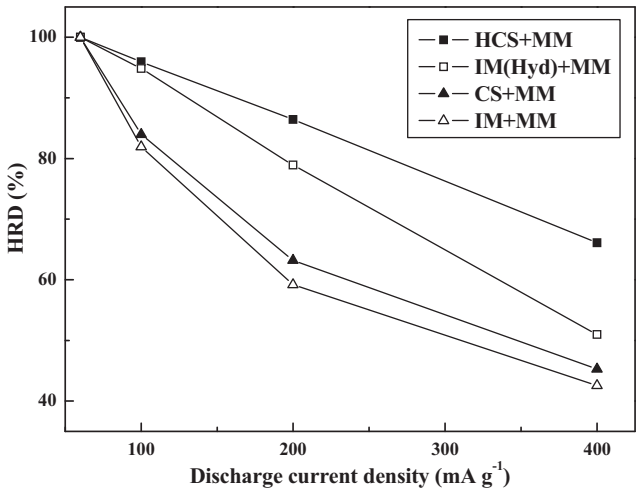

Fig. 7. High rate dischargeability (HRD) of the different samples measured at 303 K.

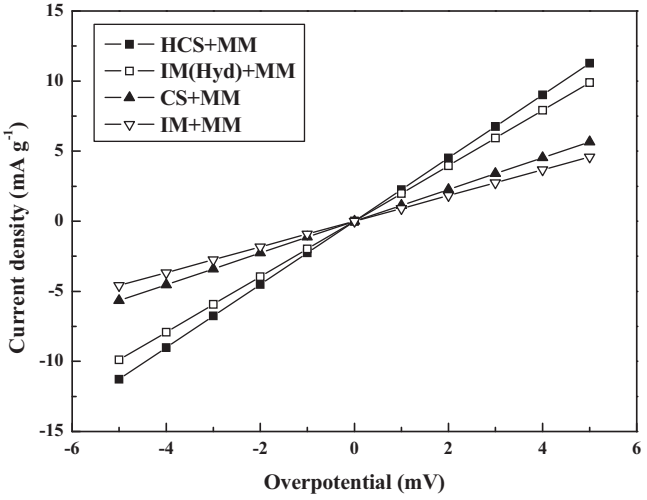

Fig. 8. Linear polarization curves of the different samples (scan rate: 0.1 mV s^{-1}).

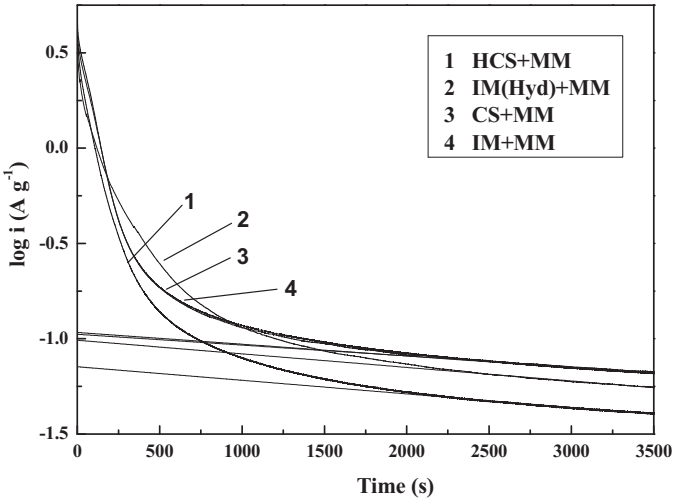

Fig. 10. Potentiostatic discharge curves of the fully charged samples (potential step: +600 mV *vs.* open circuit potential).

reactivity of the electrode during charging/discharging [45]. The results are consistent with the variation of HRD of the different electrodes.

The EIS and corresponding equivalent circuit of the different electrodes are shown in Fig. 9. It can be seen that each spectra is composed of two semicircles followed by a straight line. According to the EIS model of hydrogen storage alloy electrode [46], the high frequency semicircle, the lower frequency semicircle and the low frequency straight line are related to the contact resistance (R_c) between the current collector and the electrode pellet, the charge-transfer resistance (R_{ct}) and the Warburg impedance (W), respectively. R_s is the electrolyte resistance between the alloy electrode and the reference electrode. Constant-phase elements (CPE) are used in the equivalent circuit owing to the porosity and roughness of the electrode surface. *CPE*1 is the contact capacitance between the electrode and the current collector. *CPE*2 is the double layer capacitance. Based on the equivalent circuit and by means of non-linear least squares (NLLS) fitting of the plots, the charge-transfer resistances of the electrodes were calculated and listed in Table 1. It can be found that the R_{ct} of the HCS + MM and IM(Hyd) + MM products is much lower than that of the CS + MM and IM + MM products, and the HCS + MM product has the smallest R_{ct}, corresponding to the fastest electrochemical reaction rate on the alloy surface, which is consistent with the result obtained from the linear polarization.

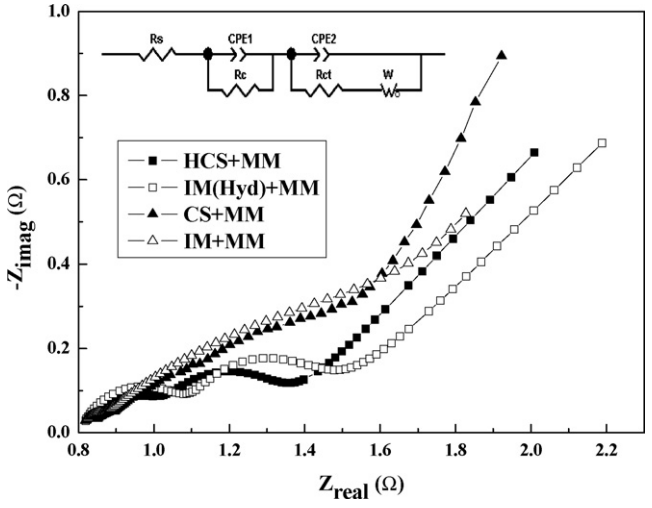

Fig. 9. Electrochemical impedance spectra and corresponding equivalent circuit of the different samples.

To investigate the hydrogen diffusion behavior in the alloys, potentiostatic discharge test was performed and the current–time responses in the semi-logarithmic plots of the different electrodes are shown in Fig. 10. The current response can be separated into two time domains [47]. One is the shorter time region (<500 s) in which the current declines sharply, and the other is the longer time region (>2000 s) in which the current decays slowly in a linear fashion. In the linear region, the hydrogen diffusion in the alloy controls the electrode process and the hydrogen diffusion ability D/a^2 can be calculated according to the following equation [48]:

$$\log i = \log\left(\pm\frac{6FD}{da^2}(C_0 - C_s)\right) - \frac{\pi^2}{2.303}\frac{D}{a^2}t \quad (3)$$

where i (A g^{-1}) is the current density, F is Faraday constant, D ($cm^2\ s^{-1}$) is the hydrogen diffusion coefficient, d (g cm^{-3}) is the density of the hydrogen storage alloy, a (cm) is the alloy particle radius, C_0 (mol cm^{-3}) is the initial hydrogen concentration in the bulk of the alloy, C_s (mol cm^{-3}) is the hydrogen concentration on the surface of the alloy particles, and t (s) is the discharge time. As the average particle size is not identical for the different samples, it is reasonable to use D/a^2 to evaluate the discharge kinetics of the electrode contributed by hydrogen diffusion. The values of D/a^2 for the different samples were determined from the slopes of linear current responses and are listed in Table 1. It can be seen that the D/a^2 value of the HCS + MM and IM(Hyd) + MM products is larger than that of the CS + MM and IM + MM products. On the one hand, the Mg_2Ni hydrides may have more nanocrystalline or amorphous phases and crystal defects after mechanical milling than the Mg_2Ni alloy [39,49]. On the other hand, the smaller particle size of the Mg_2Ni hydrides is also favorable to hydrogen diffusion. Therefore, the HCS + MM and IM(Hyd) + MM products have better hydrogen diffusion ability. As HRD is determined by both of the charge-transfer on the alloy surface and hydrogen diffusion in the alloy, it is reasonable that the HCS + MM and IM(Hyd) + MM products have better electrochemical kinetics because they have larger exchange current density I_0 and hydrogen diffusion ability D/a^2 than those of the CS + MM and IM + MM products.

In summary, both of the discharge capacity and electrochemical kinetics of the HCS + MM and IM(Hyd) + MM products are better than those of the CS + MM and IM + MM products, and the HCS + MM product exhibits the best overall electrochemical performances. Moreover, the process of HCS + MM has the advantages of short

preparation time, low energy consumption and high activity of the product as compared to the IM(Hyd) + MM process. Thus, it is suggested that HCS + MM is a promising method to prepare Mg-based hydrogen storage electrode alloy with high discharge capacity and activity.

4. Conclusions

The structural and electrochemical hydrogen storage properties of the Mg_2Ni-based alloys prepared by different methods of HCS + MM, IM(Hyd) + MM, CS + MM and IM + MM have been investigated systematically by means of XRD, SEM, galvanostatic charging/discharging and other electrochemical measurements. All the products show nanocrystalline or amorphous-like structures. The HCS + MM and IM(Hyd) + MM products have higher discharge capacity and better electrochemical kinetics property than the CS + MM and IM + MM products. The HCS + MM product possesses the best overall electrochemical performances. The process of HCS + MM is suitable for preparing Mg-based hydrogen storage electrode alloy with timesaving and energy-saving advantages. Further investigations should be focused on improving the cycling stability of the HCS + MM product.

Acknowledgements

This work was supported by National Natural Science Foundation of China (Nos. 51071085, 50871052), Natural Science Foundation of Jiangsu Province (No. BK2009361).

References

[1] J.J.G. Willems, K.H.J. Buschow, J. Less-Common Met. 129 (1987) 13.
[2] L. Schlapbach, A. Züttel, Nature 414 (2001) 353.
[3] H.G. Pan, Y.F. Zhu, M.X. Gao, Q.D. Wang, J. Electrochem. Soc. 149 (2002) A829.
[4] Y.F. Liu, Y.H. Cao, L. Huang, M.X. Gao, H.G. Pan, J. Alloys Compd. 509 (2011) 675.
[5] S. Rousselot, A. Gazeau, D. Guay, L. Roué, Electrochim. Acta 55 (2010) 611.
[6] K. Young, T. Ouchi, B. Reichman, J. Koch, M.A. Fetcenko, J. Alloys Compd. (2011), doi:10.1016/j.jallcom.2010.12.205.
[7] Y.F. Liu, H.G. Pan, M.X. Gao, Q.D. Wang, J. Mater. Chem. (2011), doi:10.1039/C0JM01921F.
[8] J. Matsuda, Y. Nakamura, E. Akiba, J. Alloys Compd. (2011), doi:10.1016/j.jallcom.2011.01.071.
[9] R.V. Denys, V.A. Yartys, J. Alloys Compd. (2010), doi:10.1016/j.jallcom.2010.11.205.
[10] H.G. Pan, R. Li, Y.F. Liu, M.X. Gao, H. Miao, Y.Q. Lei, Q.D. Wang, J. Alloys Compd. 463 (2008) 189.
[11] Q.A. Zhang, G.P. Zhao, T.Z. Si, Int. J. Hydrogen Energy 31 (2006) 1182.
[12] M.X. Gao, S.C. Zhang, H. Miao, Y.F. Liu, H.G. Pan, J. Alloys Compd. 489 (2010) 552.
[13] Q.F. Tian, Y. Zhang, L.X. Sun, F. Xu, Z.C. Tan, H.T. Yuan, J. Power Sources 158 (2006) 1463.
[14] M.X. Gao, H. Miao, Y. Zhao, Y.F. Liu, H.G. Pan, J. Alloys Compd. 484 (2009) 249.
[15] Y.F. Liu, H.G. Pan, M.X. Gao, H. Miao, Y.Q. Lei, Q.D. Wang, Int. J. Hydrogen Energy 33 (2008) 124.
[16] Y. Zhao, M.X. Gao, Y.F. Liu, L. Huang, H.G. Pan, J. Alloys Compd. 496 (2010) 454.
[17] Y.Q. Lei, Y.M. Wu, Q.M. Yang, J. Wu, Q.D. Wang, Z. Phys. Chem. 183 (1994) 379.
[18] H. Niu, D.O. Northwood, Int. J. Hydrogen Energy 27 (2002) 69.
[19] M. Anik, J. Alloys Compd. 491 (2010) 55.
[20] H.T. Yuan, L.B. Wang, R. Cao, Y.J. Wang, Y.S. Zhang, D.Y. Yan, J. Alloys Compd. 309 (2000) 208.
[21] Y.H. Zhang, B.W. Li, H.P. Ren, X.X. Ding, X.G. Liu, L.L. Chen, J. Alloys Compd. 509 (2011) 2808.
[22] M.H. Wang, L.Z. Zhang, Y. Zhang, L.X. Sun, Z.C. Tan, F. Xu, Int. J. Hydrogen Energy 31 (2006) 775.
[23] F.J. Liu, S. Suda, J. Alloys Compd. 230 (1995) 58.
[24] J. Chen, D.H. Bradhurst, S.X. Dou, H.K. Liu, J. Alloys Compd. 280 (1998) 290.
[25] J.S. Kim, C.R. Lee, J.W. Choi, S.G. Kang, J. Power Sources 104 (2002) 201.
[26] L.F. Jiao, H.T. Yuan, Y.J. Wang, Y.M. Wang, Int. J. Hydrogen Energy 34 (2009) 1476.
[27] Y.H. Zhang, L.F. Jiao, Y.J. Wang, Q.H. Wang, Y.Y. Zhang, L. Liu, H.T. Yuan, Int. J. Hydrogen Energy 33 (2008) 4819.
[28] N. Cui, B. Luan, H.J. Zhao, H.K. Liu, S.X. Dou, J. Alloys Compd. 240 (1996) 229.
[29] C.W. Hsu, S.L. Lee, R.R. Jeng, J.C. Lin, Int. J. Hydrogen Energy 32 (2007) 4907.
[30] S. Pedneault, J. Huot, L. Roué, J. Power Sources 185 (2008) 566.
[31] D.R. Leiva, R. Floriano, J. Huot, A.M. Jorge, C. Bolfarini, C.S. Kiminami, T.T. Ishikawa, W.J. Botta, J. Alloys Compd. (2011), doi:10.1016/j.jallcom.2011.01.097.
[32] K.L. Hima, B. Viswanathan, M.S. Srinivasa, J. Alloys Compd. 461 (2008) 72.
[33] T. Akiyama, H. Isogai, J. Yagi, J. Alloys Compd. 252 (1997) L1.
[34] L.Q. Li, T. Akiyama, J. Yagi, Int. J. Hydrogen Energy 26 (2001) 1035.
[35] D.M. Liu, X.F. Liu, Y.F. Zhu, L.Q. Li, J. Alloys Compd. 458 (2008) 394.
[36] S. Doppiu, L. Schultz, O. Gutfleisch, J. Alloys Compd. 427 (2007) 204.
[37] S. Mokbli, M. Abdellaoui, H. Zarrouk, M. Latroche, A. Percheron Guégan, J. Alloys Compd. 460 (2008) 432.
[38] Y. Wu, W. Han, S.X. Zhou, M.V. Lototsky, J.K. Solberg, V.A. Yarys, J. Alloys Compd. 466 (2008) 176.
[39] X.F. Liu, Y.F. Zhu, L.Q. Li, J. Alloys Compd. 425 (2006) 235.
[40] X.F. Liu, Y.F. Zhu, L.Q. Li, Int. J. Hydrogen Energy 32 (2007) 2450.
[41] A.H. Boonstra, T.N.M. Bernards, G.J.M. Lippits, J. Less-Common Met. 159 (1990) 327.
[42] Q.F. Tian, Y. Zhang, Y.X. Wu, J. Alloys Compd. 484 (2009) 763.
[43] C.S. Wang, Y.Q. Lei, Q.D. Wang, Electrochim. Acta 43 (1998) 3209.
[44] P.H.L. Notten, P. Hokkeling, J. Electrochem. Soc. 138 (1991) 1877.
[45] T. Ise, T. Nurata, Y. Hirota, M. Nogami, S. Nakahori, J. Alloys Compd. 298 (2000) 310.
[46] N. Kuriyama, T. Sakai, H. Miyamura, I. Uehara, H. Ishikawa, T. Iwasaki, J. Alloys Compd. 202 (1993) 183.
[47] T. Nishina, H. Ura, I. Uchida, J. Electrochem. Soc. 144 (1997) 1273.
[48] G. Zheng, B.N. Popov, R.E. White, J. Electrochem. Soc. 142 (1995) 2695.
[49] D.M. Liu, Y.F. Zhu, L.Q. Li, Int. J. Hydrogen Energy 32 (2007) 2417–2421.